Ultrasound in Med. & Biol. Vol. 8, No. 4, pp. 381–392, 1982
Printed in Great Britain.

0301-5629/82/040381-12$03.00/0
Pergamon Press Ltd.

AN ANTHROPOMORPHIC ULTRASOUND BREAST PHANTOM CONTAINING INTERMEDIATE-SIZED SCATTERERS

ERNEST L. MADSEN, JAMES A. ZAGZEBSKI and GARY R. FRANK
Medical Physics Department, 1300 University Avenue, Rm 1530, University of Wisconsin, Madison, WI 53706, U.S.A.

Abstract—An anthropomorphic breast phantom, built from materials which mimic tissue parenchymae with respect to attenuation coefficients, speeds of sound, densities and backscatter levels, is described in detail. One of the outstanding features of the phantom is that 30% of the volume of the glandular region consists of tissue-mimicking fat, the remainder being tissue-mimicking glandular (non-adipose) tissue. The presence of these tissue-mimicking fat globules should cause ultrasound beam distortions similar to those found in clinical scans of the breasts of younger women. Halliwell (1977) has presented direct evidence for such beam distortions in real breasts. Other tissues simulated in the phantom are: skin, subcutaneous and retromammary fat, Cooper's ligaments, ducts and (abnormal) masses. The potential areas of usefulness of the phantom are: aiding in the development of more effective ultrasound imaging machines, discovering— or verifying the causes of—various artifacts in breast imaging, routine testing of instruments being used clinically for breast imaging, and training of ultrasonographers. Ultrasound images of the phantom, made using three different instruments, are displayed and discussed.

1. INTRODUCTION

Anthropomorphic breast phantoms for use in ultrasonic imaging have been described previously (Madsen, *et al.*, 1982a). In these phantoms tissue-mimicking (TM) materials corresponding to various tissue–parenchymae (Madsen *et al.*, 1978; Madsen, 1980; Madsen *et al.*, 1982b) were employed in representative anthropomorphic configurations. In each phantom a representative breast shape is employed, and a "glandular region" surrounded by a subcutaneous fat layer is simulated. Of considerable importance for testing ultrasound imaging instruments—as well as for use in training ultrasonographers—is the fact that representative values for speeds of sound, densities and slopes of the attenuation coefficients exist in these phantoms. Thus, for example, artifacts related to refraction and reflection at the TM glandular region-to-TM subcutaneous fat layer are realistically produced. Evidence for the related significant beam distortions in real breasts exists (Halliwell, 1977).

A new anthropomorphic breast phantom is described in the present paper. The primary distinguishing feature of this phantom is the presence of spatially randomly distributed spherical TM fat globules in the glandular region. These comprise 30% of the volume of the glandular region, the remaining 70% consisting of TM non-adipose glandular tissue. These TM fat spheres range in diameter from 1.7 to 6.3 mm; thus, they are classed as intermediate-sized scatterers for ultrasonic breast imaging, although the larger ones might be classed as large particle scatterers, the latter being defined as "obstacles very much larger than the wavelength" (Wells, 1977a). The presence of such a fractional component of fat globules (30%) in the glandular region is representative of the younger breast (Greenleaf and Bahn, 1979), the effective imaging of which is of the utmost importance.

The composition and ultrasonic properties of each component TM material are presented first, followed by the gross structure of the phantom. Then ultrasound images, made with three different scanners, which are particularly suited to breast imaging, are exhibited and discussed.

2. TISSUE-MIMICKING MATERIALS

2(a) *Composition*

Four types of normal tissue are simulated: glandular, adipose, skin and Cooper's ligaments. We use the term glandular *tissue* to refer to all *normal non-adipose* tissue in the glandular *region* of the breast, the glandular region being that part of the breast containing cells capable of becoming milk-producing.

The tissue-mimicking (TM) fat appears in three forms: subcutaneous fat, retromammary fat and fat globules. All three types contain 25% olive oil and 25% kerosene, by volume. (Kerosene is a thin oil distilled from petroleum.) The remaining 50%, in the case of the subcutaneous and retromammary fat, is water-based animal hide gel. This material has been described in more detail in another publication (Madsen, *et al.*, 1982b). In the case of the TM fat globules, the remaining 50% is agar. (Agar was used instead of animal hide gelatin for manufacturing convenience.) All forms of TM fat are dispersions of microscopic droplets of the olive oil–kerosene solutions in the gel matrix; thus, they behave as elastic solids. The TM subcutaneous fat has a small added concentration of Rayleigh scatterers randomly distributed in it, enhancing Rayleigh scattering by the oil droplets themselves. These are hollow glass beads averaging 30 μm dia. and having an average density of 0.10 gm/cm^3. The TM subcutaneous fat contains 30 mg of these beads per liter.

The TM glandular tissue consists of water-based animal-hide gel with graphite particles randomly distributed in it (Madsen, *et al.*, 1978; Madsen, 1980). These particles range in diameter from 0 to 50 μm, and their concentration is 49.3 gr/l. The concentration and size distribution of these particles determine the attenuation and scattering characteristics of the TM glandular tissue *per se*.

The glandular region consists of the TM glandular tissue with spherical TM fat globules randomly distributed throughout. These TM fat spheres constitute 30% of the volume of the glandular region. These spheres were mass-produced using a technique reported elsewhere (Madsen, *et al.*, 1982c), and standard sieves were employed to allow selection of a distribution of sphere sizes for use in the phantom. The diameter distribution of the TM fat spheres contained in the glandular region is shown in Table 1.

Table 1. Diameter distribution of the TM fat spheres contained in the glandular region of the phantom

Diameter range in mm	% of the total volume of the spheres
1.7 to 2.4	22
2.4 to 3.4	22
3.4 to 4.8	45
4.8 to 6.3	11

The bulk of the TM skin consists of a random distribution of pumice powder in the water-based animal hide gel. The particles are less then 100 μm in diameter and their concentration is 95 gm/l. The scatter level for this material is higher than in the case of the TM glandular tissue. This pumice-in-gelatin layer is surrounded externally by a 0.3 mm thick soft polyethylene layer, the latter being an effective vapor barrier, an important quality for aiding in the prevention of fluid loss from the gels. The pumice-containing gelatin layer of TM skin was created inside the preformed polyethylene layer in successive sublayers; each sublayer was produced by pouring molten gelatin into the concave part of the polyethylene layer, tilting the latter at various angles until a uniform coating occurred, pouring out the excess molten galatin, and rotating about a horizontal axis for a minute or two until the gelatin congealed.

The TM Cooper's ligaments are composed of the same materials as those in the TM glandular tissue except that the concentration of graphite powder is much higher, viz. 340 gm/l. This results in a very high attenuation coefficient and a rather high density such as one might expect to find for ligaments because of their high collagen content. In producing the TM Cooper's ligaments, first a sheet of the TM material was formed between two slabs of lubricated plastic separated by 1 mm spacers. The sheet of TM material was then removed and cut into flexible strips of thickness 1 mm, widths about 1 cm and lengths 3 or 4 cm.

Four masses (volumes of abnormal tissue) are represented in the phantom. Two of these are TM cysts and consist of the water-based animal hide gelatin containing no solid or liquid particles. Another is a TM tumor consisting of the water-based animal-hide gelatin with a random distribution of graphite particles, these particles being similar to the type used in the TM glandular tissue and TM Cooper's ligaments. The concentration of graphite in this TM tumor is 94 gm/l. The remaining mass is a TM tumor consisting of a random distribution of TM fat spheres in a water-based animal hide gelatin, the latter having a graphite concentration of 175 gm/l. The TM fat spheres have the same composition as those in the glandular region, and their diameters lie between 0.9 and 1.7 mm. These fat spheres make up 30% of the volume of the TM tumor.

Except for the production of cysts, gravitationally related nonuniformities would be generated in the TM materials during congealing unless steps are taken to prevent them. This is because the small particles (graphite, pumice or oil droplets) and solid TM fat spheres have different densities than that of the water-based gels. The procedure for avoiding such nonuniformities is to rotate the TM material during congealing at 2 RPM about a horizontal axis (Madsen *et al.*, 1978). Thus, the congealed TM materials are uniform in composition except for the spatial randomness of suspended particles and TM fat spheres.

All of the gelatin in the phantom contains 4.6% *n*-propanol, 0.5% formaldehyde and 0.1% *p*-methylbenzoic acid. These materials serve as preservatives. In addition, the formaldehyde, via a phenomenon known as cross-linking, results in a melting point of the materials in the phantom in excess of 68°C. Thus, as a result of the presence of these materials, the phantom possesses permanence of its ultrasonic properties and thermal stability.

2(b). *Ultrasonic properties*

Except in the production of the TM fat spherical globules, each distinct gelatin-based TM material is formed in molds, the hot molten material congealing in the molds while being rotated, of course. For most batches of molten TM material produced, two cylindrical test samples were produced, these samples being used for measurements of ultrasonic properties. For example, when the molten TM subcutaneous fat was made, part was poured into the appropriate region of the phantom and part was poured into the cylindrical test cylinders. In the case of the material in the glandular region and in one of the TM tumors, previously solidified TM fat spheres were added to the molten TM glandular tissue before the above procedure was carried out.

The procedure used in making measurements of ultrasonic properties using the test cylinders is described in detail in one of the references (Madsen *et al.*, 1982b); error analysis methods and error estimates are also discussed there. Measurements of attenuation coefficients and speeds of sound were done using a through transmission technique. These were done at room temperature (22°C) and at a temperature typical in water bath ultrasonic scanners (34°C). Ultrasonic attenuation coefficients, α, speeds of sound, c, densities, ρ, and backscatter levels, β, relative to a perfect reflector, were measured for each component TM material. The measurements of speeds of sound were done at a frequency between 1.5 and 2.5 MHz. The attenuation coefficients were measured over the range 1.5 MHz through 6 MHz. Densities and backscatter coefficients were measured at 22°C only. Measurements of ρ and β were done only at 22°C, and β was measured for most materials at 4 MHz and for the TM subcutaneous fat and TM glandular region at 3 MHz as well as at 4 MHz. The attenuation coefficients for the TM materials used are consistently nearly proportional to the frequency (Madsen *et al.*, 1978, 1982b; Madsen, 1980). Measurements of α at 22 and 34°C for the TM material in one of the simulated tumors are shown in Fig. 1. This material consists of water-based animal hide gelatin with a graphite particle concentration of 94 gm/l.

Data for α, c, β and ρ for the various component TM materials are summarized in Table 2. Fitting of the data for α was done assuming a relation $\alpha = \alpha_0 f$ where α_0 is a constant and f is the frequency. The slopes of the attenuation coefficients, $\alpha_0 = \alpha/f$ are tabulated.

Due to the relatively large distances between the TM fat spheres of the materials composing the glandular region and the TM "high attenuation" tumor, measurement of

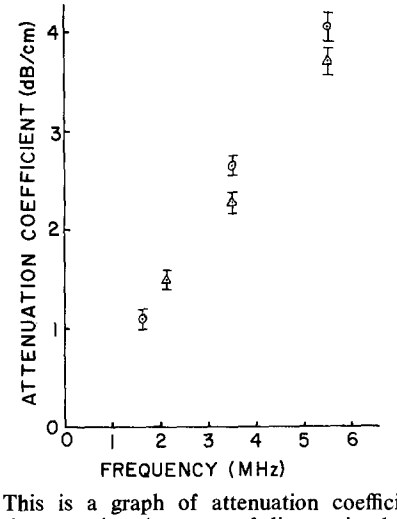

Fig. 1. This is a graph of attenuation coefficients at frequencies spanning the range of diagnostic ultrasound imaging for the TM material of which the low-scatter, irregularly shaped TM tumor is composed. One set of measurements was done at 22°C (⊙) and another at 34°C (△).

Table 2. Summary of the data for the attenuation coefficients, α, speeds of sound, c, densities, ρ, and backscatter levels, β, for the TM materials in the phantom. α and c were measured at 34°C as well as at 22°C

TM Material	22°C					34°C	
	c (m/s)	α/f (dB/cm/MHz)	ρ (gm/cm^3)	β in dB below that for a flat perfect reflector 4 MHz	3 MHz	c (m/s)	α (dB/cm/MHz)
subcutaneous fat	1462	0.40	0.94	55	62	1441	0.38
glandular tissue*	1569	0.55	1.04	45	--	1585	0.51
Fat spheres in glandular region and in high attenuation tumor	1445	0.31	0.92	not measured		1425	0.29
composite glandular region	1521±5	----	1.00	42	40	1518±5	----
irregularly shaped tumor	1566	0.74	1.07	45	--	1586	0.68
high attenuation tumor	1517±5	----	1.00	not measured		1515±5	----
skin†	1569	0.80	1.12	54 at 2.5 MHz		1586	0.73
cysts and simulated duct fluid†	1568	0.11	1.02	no scatter	no scatter	1584	0.10

*Data obtained using test cylinders made from materials identical to those in the TM glandular tissue but made at an earlier time. The reproducibility in manufacturing is approximately ±3 m/s for the speed of sound, ± 10% for attenuation coefficients, ± 0.5% for the density and ± 2 dB for the backscatter levels.

†Data corresponds to a different breast phantom reported elsewhere (Madsen, et al., 1982a). The TM skin and cysts in that phantom - and in the phantom discussed in the present paper - were made from identical materials. See footnote immediately above for reproducibility considerations.

attenuation coefficients using the test cylinders made was found to be of dubious value. Not only were large fluctuations in the transmitted signal found when the test cylinders were moved laterally, but also when moved axially with respect to the beam axis; the receiver showed variations of factors of 5 in the amplitude. Phase cancellation at 6.3 mm dia. receiving transducer probably played a significant role in producing these large fluctuations. Data for the attenuation coefficients of the TM glandular tissue and TM fat spheres, taken separately, are displayed in the table.

Measurements of speed of sound in the material composing the glandular region and TM "high attenuation" tumor were tractable, however, although the uncertainties are an order of magnitude larger than those in the case of the much more homogeneous materials.

The speeds of sound listed have been rounded off to the nearest meter per second, the uncertainty of the measurements being ± 1 m/s in all cases except those in which the TM materials contained random distributions of intermediate-sized scatterers. The latter materials are the glandular region material and the TM "high attenuation" tumor. In these cases the range in the data (not the S.D.) is shown in the table.

Two of the simulated ducts in the phantom have walls formed from 0.2 mm thick polyethylene tubing having a density of 0.92 gm/cm^3. The superficial layer of the "skin" of the phantom was formed from the same low-density type of polyethylene and has a thickness of 0.3 mm. Measurements in our laboratory on thick slab low density polyethylene yielded a density of 0.92 gm/cm^3 and a speed of sound of 2080 m/s at 22°C.

Many of the ultrasonic properties of the soft tissue parenchymae found in real breasts are not well known. The values of most of the ultrasonic properties of the TM materials in the phantom were chosen to correspond to whatever available data do exist.

For breast fat a considerable range of

speeds of sound apparently exists; values obtained via ultrasound CT range from 1390 to 1460 m/s (Greenleaf and Bahn, 1979). The speeds of sound in the TM fat types of the phantom are within this range. Other ultrasonic properties of fat are well represented (Madsen, *et al.*, 1982b).

Regarding glandular parenchyma, only guesses regarding ultrasonic properties are possible, there being no published data for breast glandular parenchyma *per se*. The speed of sound chosen for the phantom corresponds to the upper limit (1570 m/s) of the range found for whole breasts by Kossoff *et al.* (1973). Perhaps breasts exhibiting this relatively high value of speed contain little or no fat. The slope of the attenuation coefficient chosen for the TM breast glandular parenchyma is typical of that for *in vivo* human liver (Kuc *et al.*, 1981), another type of glandular parenchyma, the ultrasonic properties of which have been vigorously pursued. This is not to imply that we consider breast glandular parenchyma to be ultrasonically equivalent to liver, but the value 0.55 dB/cm/MHz for the slope of the attenuation coefficient seemed a reasonable guess, one reason being that both types of parenchymae are infiltrated with a connective tissue matrix. The densities of many non-fat-type parenchymal tissues lie in the range 1.04–1.07 gm/cm^3 (Wells, 1977b). The value of 1.04 gm/cm^3 for the TM glandular parenchyma therefore seems reasonable. The backscatter coefficients of the TM glandular parenchyma appear to be typical of those for liver for frequencies above 3 or 4 MHz (Insana *et al.*, 1982); again, no data of this type is known to exist for breast glandular parenchyma.

Skin is another tissue type for which data is sparse regarding its ultrasonic properties. The particular pumice-in-gelatin TM skin layer was chosen because its backscatter level, relative to that of other TM materials in the phantom (as observed in *B*-scans), seemed typical of that seen in *B*-scans of the real breasts, again relative backscatter levels being studied. The 0.3 mm thick polyethylene layer on the surface of the phantom manifests a speed of sound which is too high by perhaps two or 300 m/sec (see Discussion and Conclusions section).

The irregularly shaped low scatter TM tumor results in *B*-scans similar to those generated in some cases for scirrhous or medullary carcinomas (Maturo *et al.*, 1980; Wagai and Tsutsumi, 1977). Also, the speed of sound in this TM tumor is within the range found clinically for carcinomas of the breast by Greenleaf and Bahn (1979).

The other TM tumor resulted from an attempt to create intermediate particle scattering and higher attenuation relative to the surroundings. Some carcinomas cause distal shadowing, a result of higher attenuation, and heterogeneous texture patterns (Wagai and Tsutsumi, 1977), which could be associated with intermediate-sized scatterers.

3. GROSS STRUCTURE OF THE PHANTOM

3(a) *External structure*

A photograph showing the external structure of the phantom is presented in Fig. 2(a). Ultrasonic imaging is done through the superficial "outer skin" layer composed of polyethylene molded in the shape of a breast. This plastic outer skin layer protrudes from a Lucite† box having 6.3 mm thick walls. The latter box facilitates the manufacturing of the various molded internal subsections. In the lower region of the phantom an expanded stainless steel bellows can be seen. This bellows is filled with the same type of fluid used in the manufacture of the water-based gelatin found in the internal components of the phantom. The bellows and its contents form a reservoir of fluid for slowly and continuously replacing fluid lost via diffusion through the outer plastic layers.

3(b) *Internal structure*

Figure 3 shows a diagram of a sagittal section of the phantom through the nipple region. A 3 mm thick layer of gelatin, containing highly scattering pumice particles exists in contact with the outer polyethylene layer. This gelatin layer results in simulation of the relatively high scatter level of breast skin observed clinically. Internal to this skin layer is the layer of TM subcutaneous fat. The interface between this TM subcutaneous fat and the glandular region possesses undulations similar to those observed clinically, but having a rather well-defined geometry. Two of the simulated ducts, which lie nearly in this plane are seen in the glandular region. At the base of the glandular region is a disc-shaped simulated retromammary fat pad

†Lucite is a trade name for polymethyl methacrylate.

having a base 10 cm dia. and a thickness at its center of 12 mm. The flat base of the fat pad lies on a Lucite disc which forms the end of a Lucite right circular cylinder. This cylinder houses the expanded stainless steel bellows containing replacement fluid for the gels of the phantom. A hole, which is filled with a gel plug of the same TM material used in the cysts, exists in the center of the Lucite disc. The fluid in the reservoir is in direct contact with the gels of the phantom through this hole.

Figure 2(b) is a photograph of the phantom at the stage preceding the introduction of the TM Cooper's ligaments, subcutaneous fat and skin layers. The surface of the glandular region can be seen with the undulations mentioned being apparent. Most of the surface is formed of depressions having areas ranging from about 3–9 cm^2. These depressed areas have well-defined radii of curvature, the mold forming them having had a sphere 1.5 cm in radius employed in its manufacture. This geometric simplicity of the interface between the TM subcutaneous fat and TM glandular region could prove to be useful for semiquantitative analyses of image artifacts related to refraction and reflection at this interface.

A diagram of the contents of a frontal plane lying about 5 cm posterior to the nipple is shown in Fig. 4. Three of the simulated masses are spherical, having diameters as shown in the figure caption, and the fourth is irregularly shaped, having a typical diameter of about 16 mm. The TM Cooper's ligaments, which are 1 mm thick, 1 cm wide and 4 cm long, have broad surfaces which are somewhat curved and extend from the glandular region to the TM skin. In this frontal plane, minimal cross-sectional areas of these TM Cooper's ligaments exist as shown in the figure.

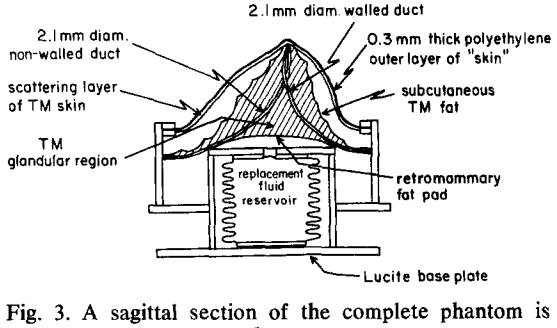

Fig. 3. A sagittal section of the complete phantom is shown.

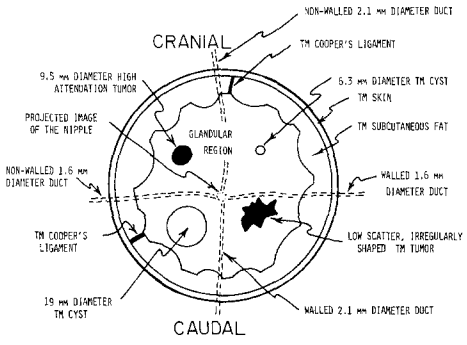

Fig. 4. This is a diagram of the contents of a frontal plane about 5 cm posterior to the nipple. The view is from the anterior. The nipple and simulated ducts do not lie in this plane, but the projection of their forms onto this frontal plane are shown with dashed lines.

4. PULSE-ECHO IMAGES OF THE PHANTOM

The phantom has been imaged using three state-of-the-art clinical instruments: the "Octoson" (Ausonics Corp.), a general purpose scanner much used for breast imaging; the "Minison" (Ausonics Corp.), a small parts scanner used principally for breast imaging; and the "Microview" (Picker) small parts scanner. The images appear in Figs. 5–13; in many cases, the figure caption provides adequate description and discussion of the image. A summary and supplementary discussion appears below.

Figures 5–8 are sector scans obtained with an Octoson, which operates at a nominal frequency of 3 MHz. Figures 9–11 were obtained with a two-transducer version of the Ausonics Minison in which the nominal frequency is 4 MHz. Figures 12 and 13 were made with the Picker Microview scanner operating at a nominal frequency of either 7 or 10 MHz.

As expected, the resolving power increases with increasing nominal frequency as one goes from 3 to 4 to 7 or 10 MHz. This statement is based in part on the capacity for imaging the TM fat spheres, or globules, in the glandular region.

Both the Octoson and the Minison exhibit depths of penetration sufficient for deep imaging for large breasts if the latter are adequately simulated by this phantom. Extensive texture fill-in is observed in the images of the retromammary fat pad, however, this effect increasing as the total pulse-echo path length through the glandular region increases. This fact strongly suggests that the fill-in is due to incident beam paths

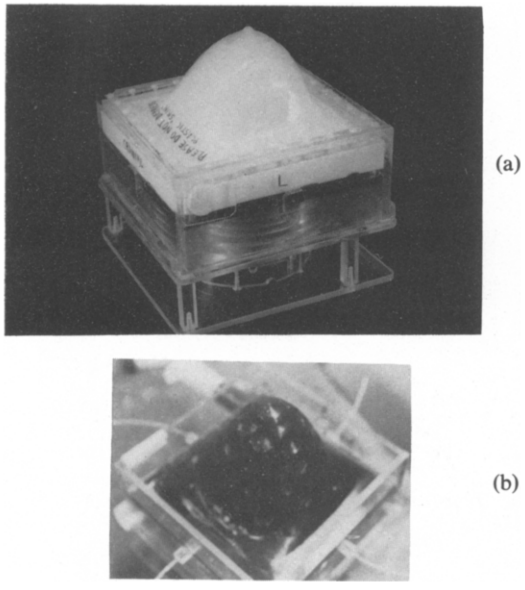

(a)

(b)

Fig. 2. A photograph of the completed phantom is shown in (a), and a photograph, taken at an intermediate stage of production is shown in (b). In (b) the surface of the glandular region to be covered by the TM subcutaneous fat is displayed; some of the TM fat spheres near the surface can be seen as light dots on the black background.

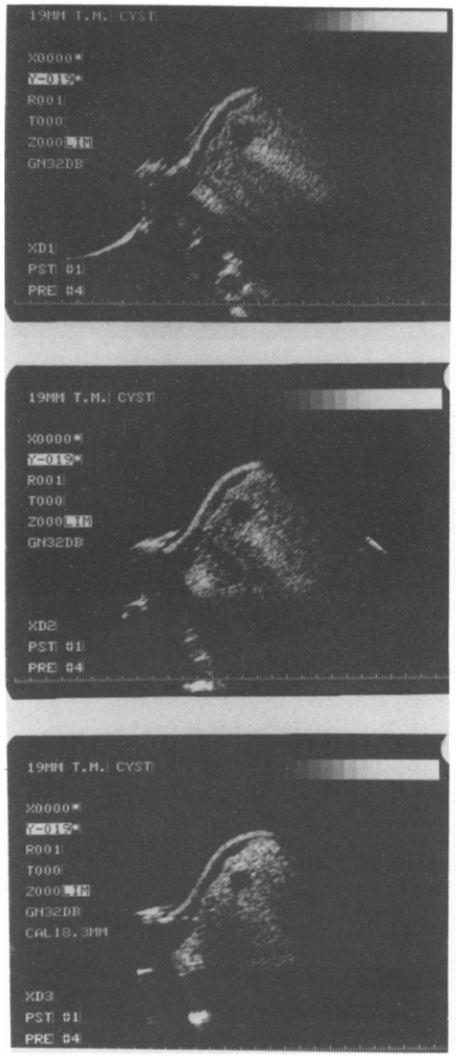

(a)

(b)

(c)

Fig. 5. Three Octoson sector scans of the same plane, which passes through the center of the 19 mm dia. TM cyst, are shown under identical conditions except that the single active transducer was different in each case; thus, the sector position varies somewhat. The position of the phantom and of the transducer bank are the same in all cases. In (a), the enhancement tail distal to the cyst is brighter and better defined than in (b) and (c); this may be due to different refraction conditions at the TM subcutaneous fat-to-glandular region interface. A puzzling chain of echoes appears diagonally 2–4 cm below the TM cyst in (b); it is absent in (a) and (c). Also in (b), well defined proximal and distal specular reflections are seen at a large fat sphere to the right of the large cyst. Premature triggering of the swept gain and strong reflections at the edge of the Lucite box are in evidence on the lower left side of each image.

Fig. 6. This is another Octoson sector scan in which the scanning plane passes through the center of the 19 mm dia. TM cyst; however, this scanning plane is at right angles to that used in obtaining the images in Fig. 5. The enhancement tail distal to the large TM cyst is large and well defined, and appears to extend through the very low scatter TM retromammary fat pad along with neighboring backscatter texture associated with the glandular region. (The region of the retromammay fat pad is between the arrows.) This fill-in of the TM retromammary fat pad may result from increased path lengths arising from cumulative deviations of beam and echo paths associated with the presence of the fat spheres.

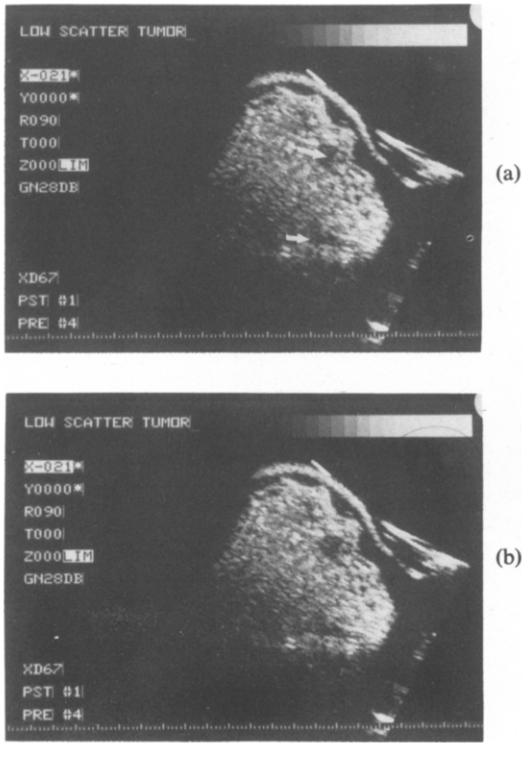

Fig. 7. These are identical photographs of a sector scan made with the Octoson. The upper image has arrows designating two structures: the upper arrow designates the image of the irregularly shaped, low-scatter-level TM tumor and the lower arrow designates the image of a part of the TM retromammary fat pad. Shadowing or enhancement distal to the TM tumor is not detectable.

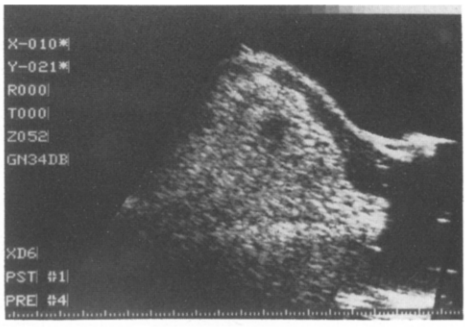

Fig. 8. This is another Octoson sector scan through the irregularly shaped, low-scatter-level TM tumor. The scanning plane is at 90° to that involved in Fig. 7. A slight shadowing distal to the TM tumor may exist.

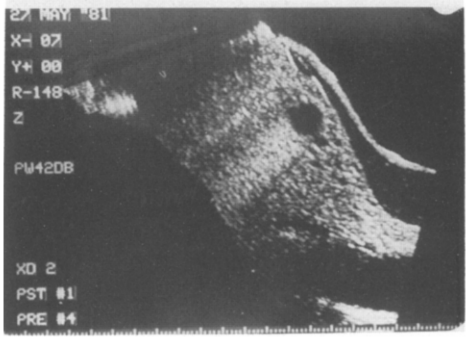

Fig. 9. This is a single transducer scan made through the 19 mm dia. TM cyst with the Minison (Ausonics Corp.). The transducer operates with a nominal frequency of 4 MHz. The resolution of the fat spheres may be somewhat better here than in the Octoson images.

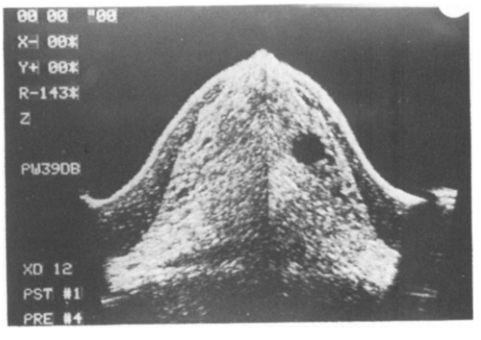

Fig. 10. This is a two transducer Minison scan in which two sector scans are imaged adjacent to one another; thus, this is *not* a compound scan. Perhaps different sensitivity settings from those in the case of Fig. 9 have resulted in a higher apparent relative scatter level in the subcutaneous fat compared to that seen in Fig. 9. On the same horizontal level with the 19 mm cyst, but near the other side of the glandular region, is seen either the small 6.3 mm dia. TM cyst or a larger fat sphere. The small TM cyst should be close to this position; however, the imaged specular reflection on the distal side of the cyst-like object indicates that this is a large fat sphere. Notice that the retromammary fat pad is better defined than in the case of the Octoson scans.

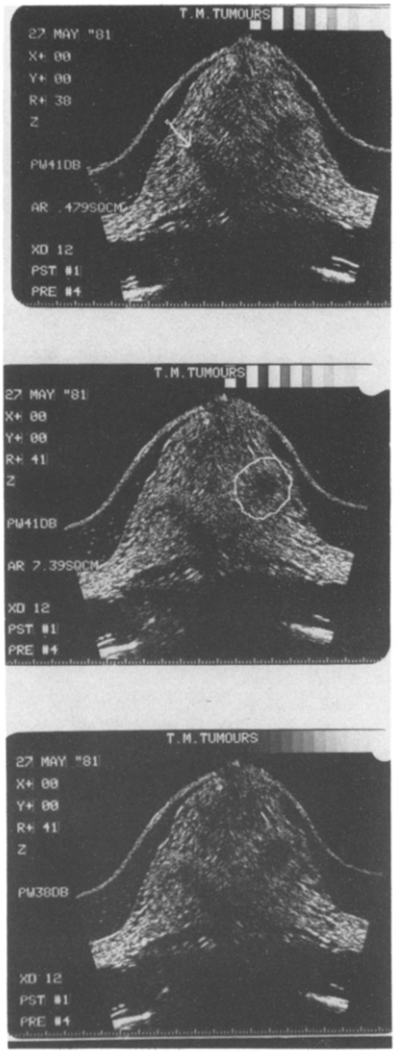

Fig. 11. These are nearly identical Minison scans. (a) and (b) were done with the same instrument power settings. (c) was done with 3 dB less power, but otherwise is identical to (b). The scanning plane of (a) was rotated 2° about the central vertical axis with respect to the scanning plane in (b) and (c); thus, the image features of (a) are slightly different. The arrow in (a) designates the distal surface of the 9.5 mm dia., high attenuation TM tumor and the proximal end of the associated shadow; the head of the arrow lies over the image of the high attenuation tumor itself. The texture pattern of this higher attenuation TM tumor has about the same "brightness level" as that of the surrounding glandular region. However, the texture should be—and probably is—more uniform than in the glandular region because of the smaller diameter distribution of the TM fat spheres in this tumor compared to that in the glandular region. The TM tumor is too small, however, to make this texture uniformity comparison a definite observation. The circle in (b) outlines the region in which the low scatter, irregularly shaped TM tumor has been imaged. This TM tumor is not as well defined as in the scans with the 3 MHz Octoson (see Fig. 7).

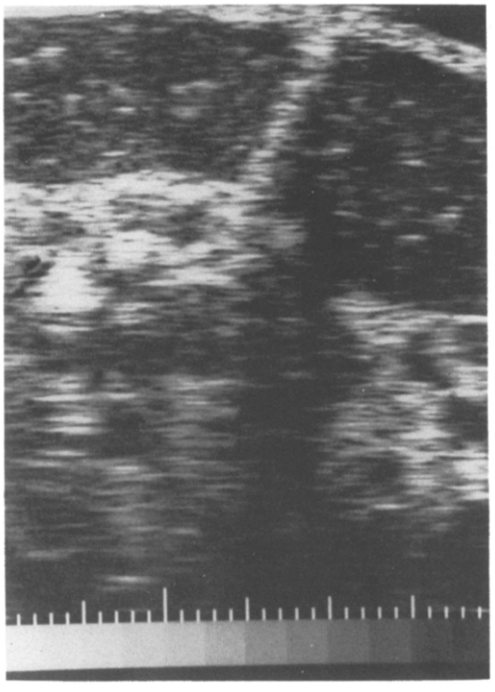

Fig. 13. This shows an image made with the Picker Microview scanner at a nominal frequency of 10 MHz. A TM Cooper's ligament is seen extending through the subcutaneous fat from the glandular region to the TM skin; the scanning plane is perpendicular to the TM Cooper's ligament so that the 1 mm thickness of the latter is demonstrated. Shadowing related to the TM Cooper's ligament is apparent.

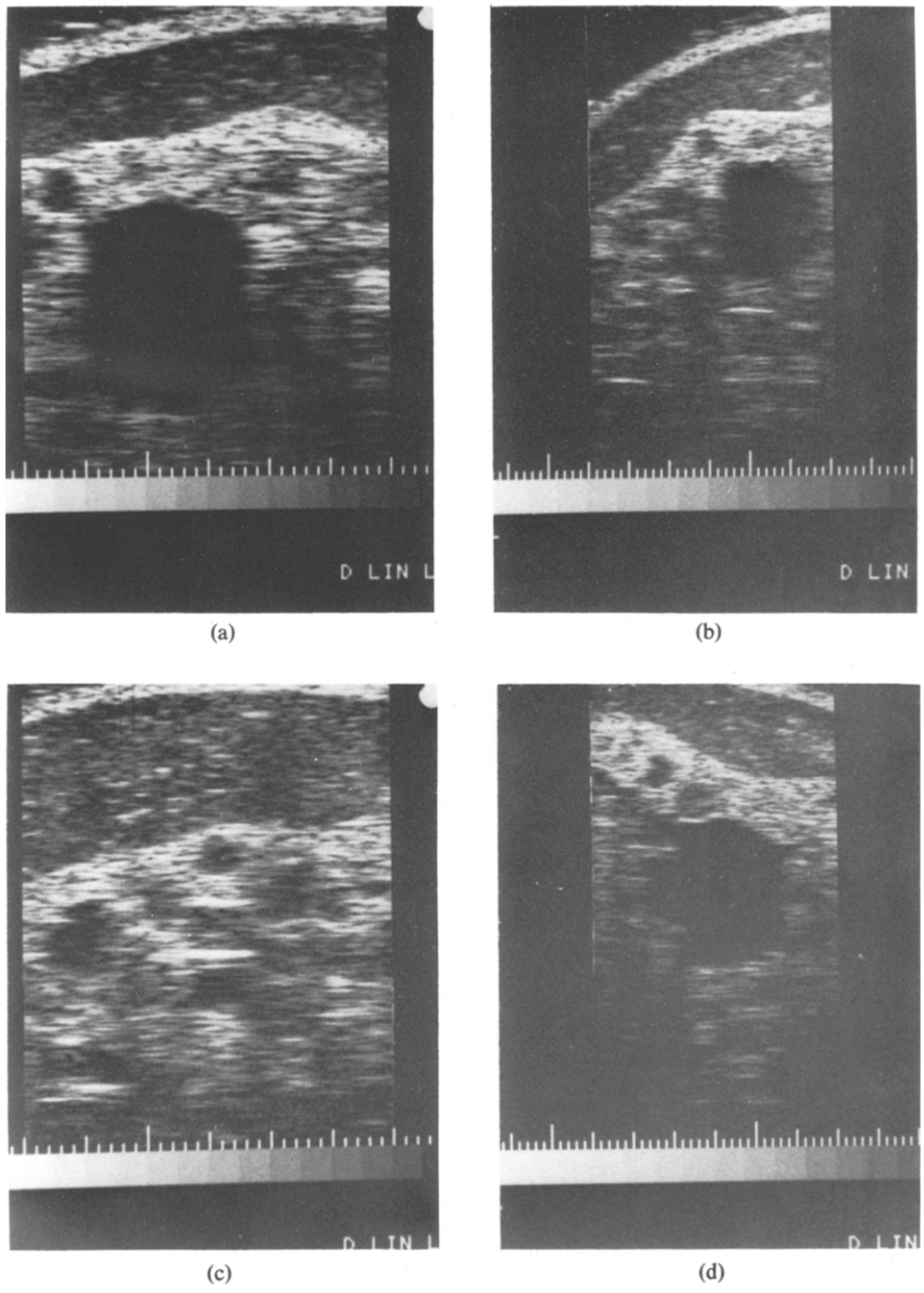

Fig. 12. These are four images made with the Picker Microview scanner. The smallest increments on the displayed horizontal scale are 1 mm. The two images on the left are at a nominal frequency of 10 MHz and those on the right are at 7 MHz. In each image the TM skin is uppermost covering the TM subcutaneous fat beneath which is the glandular region. Many TM fat spheres in the glandular region have been resolved. In (a), (b) and (c) the 19 mm dia. cyst was imaged. In (a) the imaged cyst measures about 17 mm vertically and 12 or 13 mm horizontally. Notice two of the large fat spheres (smaller low echo regions), one to the upper left of the cyst and one to the upper right of the cyst; these fat globules seem to be associated with chains of echoes distal to them causing the cyst's image to be nonspherical because its lateral extents have been masked. These distal echoes may result from refraction and/or reflection effects causing echoes from glandular region scatterers to be displayed distal to the fat spheres. In (b) and (c) the 19 mm dia. cyst is shown again, the nominal frequency being 7 MHz. Except for its left side, the spherical shape of the TM cyst is defined. In (d) an image at 10 MHz is shown of a region not containing a simulated mass. Notice the decrease with depth of the quality of definition of the fat spheres in the glandular region; this is due to the attenuation of the peak amplitudes of echoes and—perhaps to some extent—to pulse and echo "beam hardening" effects resulting in lowering of the effective interrogation frequency. The depth of penetration along paths not including the 19 mm dia. cyst is about 4 cm in all four of the images.

and returning echo pulse paths not being essentially straight lines, a condition created by the presence of the randomly distributed fat spheres: the greater the distance travelled in the glandular region, the more encounters with fat spheres and the more severe this "pulse-echo straggling" is. The result on the image is that the machine will map an echo at a deeper position than that of the echo source.

For this phantom the depth of penetration for the Picker Microview machines is estimated to be about 4 cm whether the nominal frequency is 7 or 10 MHz. Conceivably, the echoes returning from the deepest scatterers have carrier frequencies in the 4–5 MHz range for both the 7 and 10 MHz input pulses. This would result from "beam hardening" meaning the preferential attenuation of the higher frequency components in the broad band pulses with the concomitant enhanced penetrating ability of the pulses (beam).† Such lowering of the carrier frequencies also reduces lateral resolution resulting in a reduced capacity for imaging smaller TM fat spheres at depth.

Another phenomenon which is manifested is the frequency dependence of scattering as a function of the scattering particle's diameter. Particles which are small compared to the wave length scatter sound waves such that the scattered *amplitude* is proportional to the square of the frequency (Rayleigh scattering). As the size of the scatterer gets larger, this frequency dependence diminishes until it disappears entirely for scatterers having radii of curvature which are much larger than the wavelength. The TM fat spheres in the glandular region are classed as intermediate sized scatterers or, particularly perhaps with respect to higher frequencies and larger TM fat spheres, as large-sized scatterers. Four TM materials in the phantom in which Rayleigh (or small) scatterers are the source of echoes are: the TM glandular tissue surrounding the TM fat spheres and forming 70% of the volume of the glandular region, the TM subcutaneous fat, the irregularly-shaped low scatter TM tumor, and the TM fat making up the fat spheres. (The scatter level due to the oil droplets in the latter was considered to be far enough below that for the other three that measurements of scatter level were not made for this material.) In the glandular region the scatter signals are a blend of Rayleigh scattering from the graphite particles in the TM glandular tissue and intermediate and large particle scattering from the TM fat spheres. Thus, as the beam nominal frequency increases, the difference in scattered amplitudes between echoes arising in the subcutaneous fat and in the glandular region should decrease. For example, examination of Figs. 7, 9 and 12 tends to corroborate this diminishing difference in texture brightness with increasing frequency, particularly when the 7 and 10 MHz scans in Fig. 12 are compared to those at 3 and 4 MHz in Figs. 7 and 9. The scan in Fig. 10 in which the nominal transducer frequency is 4 MHz seems to disagree with this idea, the difference in texture brightnesses being similar to that in Fig. 12. This is likely due to the distinction between grey levels at the higher echo amplitude end of the amplitude range being diminished (a grey-scale saturation effect). Thus, echo signal amplitude variations resulting from Rayleigh scattering and those from intermediate particle scattering are much less distinguishable in this image than in the other images (figures) mentioned.

The same phenomenon should apply to a comparison of the frequency dependence of the distinguishability of the irregularly shaped, low-scatter-level TM tumor. The 3 MHz Octoson creates more distinct images of this TM tumor (Figs. 7 and 8) than in the case of the 4 MHz Minison (Fig. 11). Even when different machine power levels are used, the distinction between the TM tumor and its surroundings—on the basis of texture brightness—does not appear to be as good as in the case of the Octoson (compare Figs. 11(b) and (c) with Figs. 7 and 8).

5. DISCUSSION AND CONCLUSIONS

This phantom takes another step in the direction of producing realistic breast phantoms for use in quantitative testing of state-of-the-art ultrasound imaging machines and for use in training ultrasonographers in the

†The term "beam hardening" is one used in clinical radiology which refers to the decrease in a beam's effective attenuation constant which accompanies the filtering out of more highly attenuatable components. Whether the latter components are higher or lower frequencies is not relevant. In the case of diagnostic ultrasound beams (and, also for γ-ray beams above 5 MeV in lead), the higher frequency components are preferentially filtered out. Use of the term "beam hardening" in diagnostic ultrasound by physicists and engineers should promote effective communication with radiologists and clinical technologists.

effective use of clinical machines for breast imaging. The most important advance embodied in this phantom compared to those reported earlier (Madsen *et al.*, 1982a) is the incorporation of intermediate (and large) sized scattering tissue-mimicking fat spheres, or clumps, in the glandular region. The presence of such fat clumps exists in real breasts and, thus, might produce effects similar to those observed in this phantom. A ratio of 30% fat to 70% nonfat tissue in the glandular region is representative of the situation in younger breasts, effective ultrasound imaging of which is of primary importance.

Simulated ducts equivalent to those in this phantom can be imaged with ordinary *B*-scanners when those ducts are embedded in TM glandular parenchyma only. It may be that the large scale beam deviating quality of the TM fat spheres in the phantom is responsible for the inability of the diagnostic ultrasound instruments to image the four simulated ducts in the phantom. Resolution capabilities of imaging machines should be tested using such realistic phantoms rather than simple homogeneous phantoms. The largest diameter of the simulated ducts is 2.1 mm. Perhaps it is unrealistic to expect ducts this small in diameter to be imaged. Future phantoms will contain ducts of larger diameters.

A disadvantage of the external 0.3 mm thick polyethylene layer of the TM skin is that its presence results in a critical angle, relative to pulses incident from the bathing water, which is less than that observed in clinical breast scans. The critical angle for the phantom is about 45° as can be seen in Figs. 5(a)–(c). The critical angle observed in clinical breast scans is about 60°. Tests are being done to determine the advantages and disadvantages of using a molded polyurethane layer in place of the polyethylene layer. Polyurethane has been recommended as a skin-mimicking material (Carson, 1980); probably its main advantage is its lower speed of sound which yields a larger critical angle.

Two of the primary values of anthropomorphic breast phantoms such as that described in this paper are: (1) ultrasonic properties are precisely known and representative of those in tissues forming breasts, and (2) the shapes and sizes of the various simulated parenchymal tissues are representative of those in real breasts. Therefore, the extent to which a diagnostic ultrasound instrument can determine *a priori* the sizes, shapes, and ultrasonic properties of the structures in the phantom may prove to be a strong measure of the instrument's diagnostic effectiveness.

Acknowledgements—The authors are greatly indebted to Raymond L. Wood for using the phantom to obtain the images on three different ultrasound imaging instruments suited to breast imaging. Gratitude is also extended to Orlando Canto for his expeditious generation of the high quality figures and to Anne Zimmerman and Colleen Schutz for their typing proficiency and high level of accuracy.

This work was supported by NCI grants 5-P01-CA-19278 and 5-R01-CA-25634.

REFERENCES

Carson P. L. (1979) Private communication.

Greenleaf J. and Bahn R. (1979) Private communication.

Halliwell M. (1977) Ultrasonic beam distortion by the normal human breast. *Proc. and Abstracts of the 22nd Annual Meeting of the Americal Institute of Ultrasound in Medicine*, p. 94. Dallas, Texas.

Insana M. F., Zagzebski J. A. and Madsen E. L. (1982) Acoustic backscattering from ultrasonically tissue-like media. Submitted to *Med. Phys.*

Kossoff G., Fry E. K. and Jellins J. (1973) Average velocity of ultrasound in the human female breast. *J. Acoust. Soc. Am.* **53**, 1730–1736.

Madsen E. L., Zagzebski J. A., Banjavic R. A. and Jutila R. E. (1978) Tissue-mimicking materials for ultrasound phantoms. *Med. Phys.* **5**, 391–394.

Madsen E. L. (1980) Ultrasonically soft tissue mimicking materials. In *Medical Physics of CT and Ultrasound: Tissue Imaging and Characterization* (Edited by G. D. Fullerton and J. A. Zagzebski, pp. 531–550. American Institute of Physics, New York.

Madsen E. L., Zagzebski J. A., Frank G. R., Greenleaf J. F. and Carson P. L. (1982a) Anthropomorphic breast phantoms for assessing ultrasonic imaging system performance and for training ultrasonographers: I and II. *J. Clinical Ultrasound.* **10**, 67–75 and 91–100.

Madsen E. L., Zagzebski J. A. and Frank G. R. (1982b) Oil-in-gelatin dispersions for use as ultrasonically tissue-mimicking materials. *Ultrasound Med. Biol.* in press.

Madsen E. L., Zagzebski J. A., Insana M., Burke T. and Frank G. R. (1982c) Ultrasonically tissue-mimicking liver including the frequency dependence of scatter. *Med. Phys.*—submitted.

Maturo V., Zusmer N., Gilson A., *et al.* (1980) Ultrasound of the whole breast utilizing a dedicated automated breast scanner. *Radiology* **137**, 457–463.

Wagai T. and Tsutsumi M. (1977) Ultrasound examination of the breast. In *Breast Carcinoma, the Radiologist's Expanded Role*, (Edited by W. W. Logan), pp. 325–342. Wiley, New York.

Wells P. N. T. (1977a) *Biomedical Ultrasonics*, p. 43. Academic Press, London.

Wells P. N. T. (1979b) *Biomedical Ultrasonics*, p. 136. Academic Press, London.